Counter-propagating waves enhance maneuverability and stability: a bio-inspired strategy for robotic ribbon-fin propulsion

Shahin Sefati, Izaak Neveln, Malcolm A. MacIver, Eric S. Fortune and Noah J. Cowan

***Abstract*— Weakly electric knifefish, *Eigenmannia*, are highly maneuverable swimmers. The animals rely on a long, undulating ribbon fin to generate propulsive force. During closed-loop control of hovering and station keeping, knifefish partition their fin to produce two inward counter-propagating waves, enabling them to hover and rapidly change direction. In response to moving objects or changes in ambient flow speed, the fish can actively modulate the nodal point where the two waves meet. During hovering, this nodal point is somewhere in the middle, but it can be moved forward or backward changing the relative force generated by the front and back portions of the fin. Although this strategy for thrust generation may be energetically inefficient, we show here that it enables rapid switching of swimming direction and produces a linear drag-like force that confers passive stability. Robotic results and simple computational simulations reveal that the net force generated by counter-propagating waves changes linearly with respect to the nodal position. Another strategy for reversing swim direction would be to completely reverse the direction of a single traveling wave. We show why full wave reversal (and similar strategies) may be ineffective for low-speed swimming—a regime where counter-propagating waves may simplify control.**

I. INTRODUCTION

Weakly electric knifefish, such as the glass knifefish *Eigenmannia virescens* Fig. 1(A) are excellent model systems for the study of locomotion mechanics [4], [5], [10], sensing [11], [17] and neural control [14].

A better understanding of locomotor mechanics is essential for studying sensory systems and control [3], [11]. *Eigenmannia* exhibit gymnotiform locomotion in which a long undulatory ribbon-fin along the body generates thrust while the body is held rigid [10]. Although some species tend to produce a single traveling wave along their fin, *Eigenmannia* routinely employs two counter-propagating waves, one from head to tail and one from tail to head. These two waves meet at a point somewhere along the fin which we call the *nodal point*.

It is important to recognize that the entire ribbon fin is actuated by muscles along the length of the body, so the traveling wave is not the result of a passive mechanical propagation (as with sound or water waves). Rather, traveling waves on the fin likely reflects the production of traveling waves of muscle activation along the body of the fish.

S. Sefati and N. J. Cowan are with department of Mechanical Engineering, Johns Hopkins University, Baltimore MD, USA (shahin@jhu.edu)

E. S. Fortune is with department of Psychology and Brain Sciences, Johns Hopkins University, Baltimore MD, USA

I. Neveln and M. A. MacIver are with department of Mechanical Engineering and department of Biomedical Engineering, Northwestern University, Evanston IL , USA

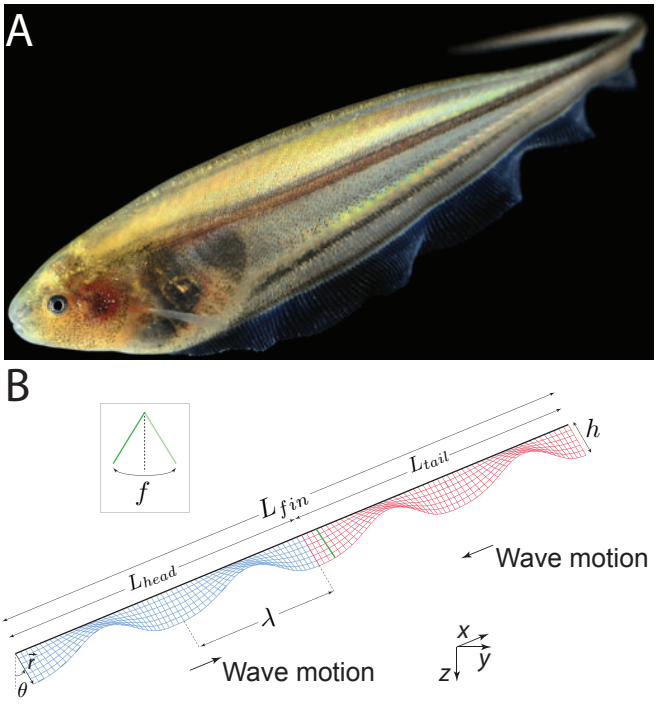

Fig. 1. Photograph of the weakly electric fish and schematic of fin kinematics. (A) Weakly electric knifefish *Eigenmannia virescens*. (B) Schematic of the fin kinematics including angular amplitude (θ), frequency (f), wavelength (λ), fin height (h), lengths of two counter-propagating waves (L_{head} and L_{tail}) and the reference frame (0 at center of the fin, negative x toward tail, *surge* force in x direction).

Since there are ≈ 100 actuated fin rays, ribbon-fin control suffers from the degrees-of-freedom problem [2]. In principle, only six degrees of forces and torques are required for all possible forces and torques on the body for maneuvering. How might the excess fin degrees of freedom be collapsed for control?

Counter propagating waves—which require just a few parameters to describe—may be an effective strategy for solving the degrees-of-freedom problem, as well as conferring stability and maneuverability to the animal. In addition to the nodal point (where the two waves meet), the fish can modulate a variety of fin kinematic parameters to vary thrust Fig. 1(B). The ribbon fin consists of rays that are spaced about a millimeter apart. These rays oscillate with a phase lead or lag relative to adjacent rays to produce a traveling wave along the body. The kinematic parameters of the traveling wave include wavelength (λ), temporal frequency (f), angular oscillation amplitude (θ), height of the fin (h) and length of the fin (L). Among these parameters,

height and length are morphological parameters that can not be controlled actively by fish. For species that produce two counter-propagating waves, fin lengths of the individual traveling waves can also be actively controlled by the fish, although total fin length does not change.

The two waves meet at a nodal point that is somewhere in the middle of the fin while the fish is hovering. As we show in this paper, the fish can directly manipulate the position of nodal point as an effective strategy for fore-aft swimming, reducing the high dimensional control problem to a single control variable.

Using counter-propagating waves bears an energetic cost: when stationary, the animal consumes metabolic energy to produce antagonistic forces that cancel each other, producing no net thrust. What might be the advantage of producing two counter-propagating waves along the fin?

In this study, we addressed this question by examining the role that the position of the nodal point plays in the generation of fore-aft forces. We examined the kinematics of *Eigenmannia* in a station-keeping behavior. Based on this kinematic data, we developed a simplified model of the fluid mechanics, and used the model to predict the forces generated by counter propagating waves under a variety of conditions. We tested the model using a robotic ribbon-fin system, equipped with force sensors to measure net force on the fin. Both numerical and experimental results reveal that counter-propagating waves can enhance maneuverability and stability, at the expense of energy.

II. METHODS

A. Biological experiments

All procedures using vertebrate animals were reviewed and approved by the Johns Hopkins University animal care and use committee and follow guidelines established by the National Research Council, the Society for Neuroscience, and previously established methodologies [9].

1) Experimental setup: tunnel Fig. 2(A). Fish naturally tend to swim into and stay within the tube, apparently using it as a refuge [3], [13]. As the flow speed is changed, the fish modulates its motor behavior to remain stationary relative to the PVC refuge. The flow tunnel was 90 cm long, 25 cm wide, and 30 cm deep. The flow speed was adjusted using the frequency setting of an electric pump which circulated water through the flow tunnel. The PVC tube was 15 cm long with the bottom milled away to allow high-speed videography of fin motion from beneath the test section. Mean and standard deviation of fin lengths of five individuals in the experiment were 7.35 cm and 0.56 cm.

2) Experiments: Individual fish ($N = 5$) were placed in the flow tunnel. Water was maintained at approximately 25° C. Each experiment consisted of nine trials with varying flow speeds from 0 to 12 cm/s in 1.5 cm/s increments. The order of the applied flow speeds was randomized in each set of data and three replicates (sets) of data were collected for each individual. The fish were given ample time to rest between trials.

For each trial, several seconds of data were collected. Using MATLAB code [7], the position of the fish was tracked from the video and one second of data (100 frames) of steady state swimming was selected for quantifying the fin kinematic parameters. Nodal position and positions of both ends of the fin were tracked from the data using custom MATLAB code.

B. Numerical simulation

1) Fin model: The ribbon fin consists of several rays along the bottom of the body. These rays oscillate out of phase thus the whole fin motion can be modeled ideally as two sine waves propagating in opposite directions:

$$\theta_t(x,t) = \theta_{max} \sin 2\pi\Big(\frac{x}{\lambda_t} + f_t t\Big), \tag{1}$$

$$\theta_h(x,t) = \theta_{max} \sin 2\pi\Big(\frac{x}{\lambda_h} - f_h t\Big). \tag{2}$$

where indices t and h refer to tail and head waves. All kinematic parameters are shown in Fig. 1(B). The base of the fin ($\|r\| = 0$) has no movement and instantaneous velocity of each point on the ray is equal to the distance from base of the fin times the angular velocity:

$$u_{\text{fin}} = r_m \frac{\partial\theta}{\partial t}\big(\sin\theta\vec{\mathbf{j}} + \cos\theta\vec{\mathbf{k}}\big). \tag{3}$$

2) Drag model: The computational model used in this paper is based on a fluid drag model. This model has been used in numerous numerical analysis [6], [12], [15], [16]. The model matches experimental data well when flow regime has high Reynolds number and neglects the fluid interaction. Under the conditions of the experiment, the Reynolds number ($Re = \frac{UL}{\nu}$) can be estimated in the range of 10^3 to 10^4 ($\nu_{\text{water}} = 10^{-6}$ m^2/s, $L_{\text{fin}} \sim 0.1$ m, for $U \sim 1 - 10$ cm/s). We created a mesh of cells on the fin and each square cell is like a flat plate moving against the flow. The drag force applied to the each propulsive element is given by:

$$d\vec{\mathbf{F}} = \frac{1}{2} C_D \rho dA[\mathbf{U}\cdot\mathbf{n}]^2\mathbf{n} \tag{4}$$

where C_D is the coefficient of the drag depending on the shape, ρ is the density of the fluid, dA is the area of the element and $\mathbf{U}$ is the velocity of the center of each element relative to the fluid and $\mathbf{n}$ is the unit normal vector to the surface. The coefficient of drag for a flat plate moving normal to the fluid is $C_D = 1.28$ [1]. The instantaneous net force is computed by integrating infinitesimal forces of all elements. The instantaneous net force of all the elements is then integrated over time for on fin cycle to compute the average propulsive force.

For a single propagating wave, assuming frequency, wavelength, angular amplitude and height of the fin remain constant along the fin, the above model can be further reduced as follows:

$$F = aL\mathbf{U} = aL(\vec{V}_{\text{wave}} - \vec{U}_{\text{fish}})^2, \tag{5}$$

where a is a constant, L is the whole length of the fin, U_{fish} is the fish steady state swimming velocity and $V_{\text{wave}} = \lambda f$ is the wave speed of the traveling wave along the fin.

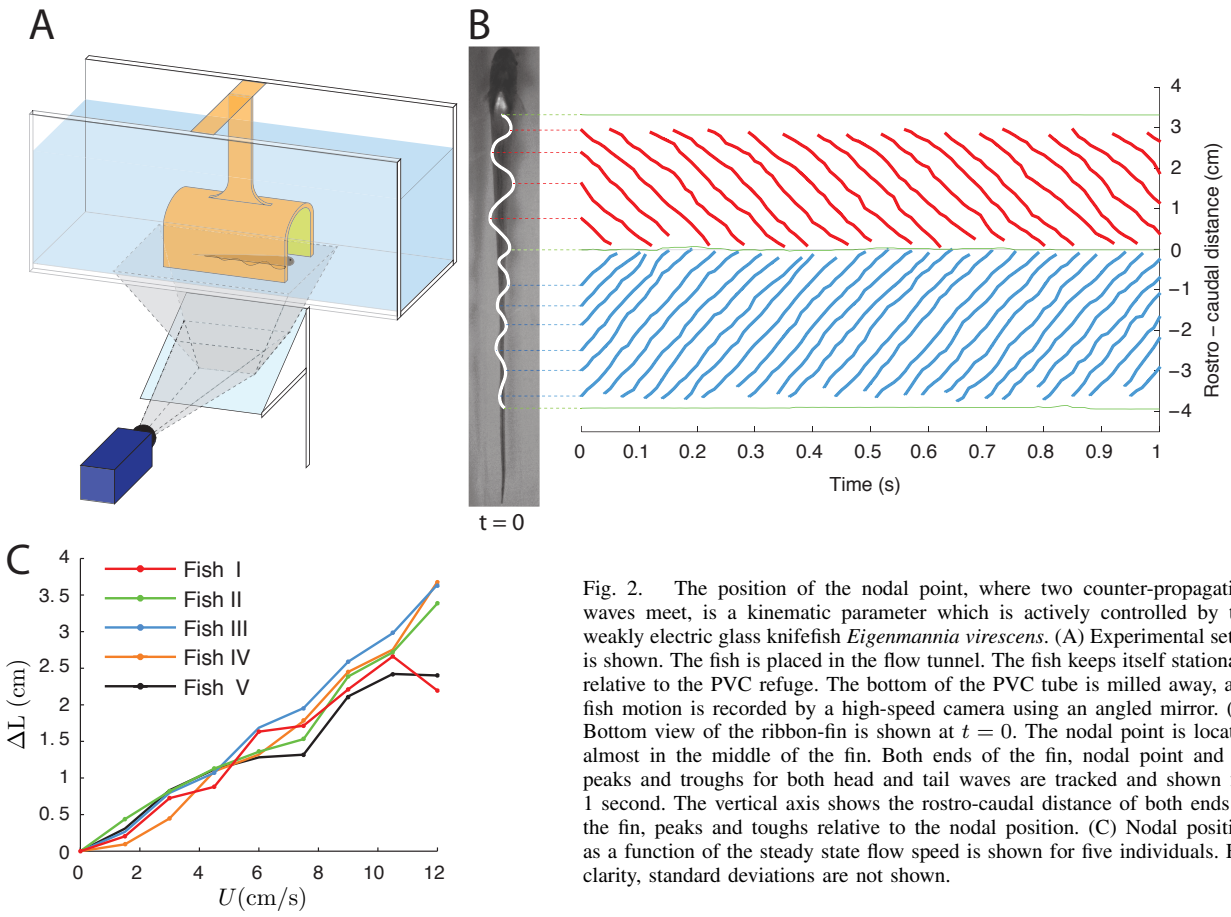

Fig. 2. The position of the nodal point, where two counter-propagating waves meet, is a kinematic parameter which is actively controlled by the weakly electric glass knifefish *Eigenmannia virescens*. (A) Experimental setup is shown. The fish is placed in the flow tunnel. The fish keeps itself stationary relative to the PVC refuge. The bottom of the PVC tube is milled away, and fish motion is recorded by a high-speed camera using an angled mirror. (B) Bottom view of the ribbon-fin is shown at $t = 0$. The nodal point is located almost in the middle of the fin. Both ends of the fin, nodal point and all peaks and troughs for both head and tail waves are tracked and shown for 1 second. The vertical axis shows the rostro-caudal distance of both ends of the fin, peaks and toughs relative to the nodal position. (C) Nodal position as a function of the steady state flow speed is shown for five individuals. For clarity, standard deviations are not shown.

If the fin is divided into two counter-propagating waves, one of length $L/2+\Delta L$ and one of length $L/2-\Delta L$, where ΔL is the nodal shift from the middle of the fin (positive ΔL means the nodal point is toward the tail from the fin mid-point), then the net thrust generated by the two counter-propagating waves is proportional to

$$F_{\text{fin}} \propto \left(\frac{L}{2}+\Delta L\right)(V_{\text{wave}}-U_{\text{fish}})^2 - \left(\frac{L}{2}-\Delta L\right)(V_{\text{wave}}+U_{\text{fish}})^2. \quad (6)$$

Assuming all the kinematics parameters of the fin except nodal shift are held fixed it is easy to show that

$$F_{\text{Fin}} = (\kappa+\gamma U_{\text{fish}}^2)\Delta L - \beta U_{\text{fish}}. \quad (7)$$

where $\kappa = 2aV_{\text{wave}}^2$, $\gamma = 2a$ and $\beta = 2aLV_{\text{wave}}$ and a is a constant.

C. Biologically inspired robotic fish

Using a biomimetic knifefish robot [4], [5], we experimented over a range of selected fin parameters while directly measuring the force generated by the counter-propagating waves of the ribbon-fin. The fin was 3.37 cm deep and 32.60 cm long, and it consisted of 32 rays which are each individually actuated by 10 mm servo motors (RE10, Maxon Motor AG, Sashsein, Switzerland) with a rated torque of 50 mN m. Control of these motors was achieved through a microcontroller running embedded LUA over a controller area network (CAN) bus, which interfaced with a custom Matlab front end allowing us to adjust the undulation frequency, fin wavelength, angular amplitude, and nodal point of the counter-propagating waves for each trial [4], [5].

We performed two experiments measuring the force generated by the robot to compare with the simulations using the fish fin kinematics. In each case, we suspended the knifefish robot from a low friction air bushing platform into a flow tunnel tank 80 cm long, 33 cm wide, and 28 cm deep. The platform was fixed in the transverse direction, and a 9 N single axis force sensor (Futek Advanced Senor Technology, Irvine, CA, USA) was attached between the platform and mechanical ground in the fore-aft direction, allowing for measurement of surge force of the robot. Voltage readings were collected at 1000 Hz using a data acquisition system (NI USB-2619, National Instruments Corporation, Austin, TX, USA), converted to force units, and averaged over 5 seconds after transient startup forces had passed.

In the first experiment we varied the nodal point of the counter-propagating wave in increments of 1.63 cm from -8.15 cm to 8.15 cm in standing water and measured longitudinal (fore-aft) force. We repeated this experiment over a range of fin oscillation frequencies (for 1, 2, 3 and 4 Hz), and angular amplitudes (for 20°, 25° and 30°) (Table I).

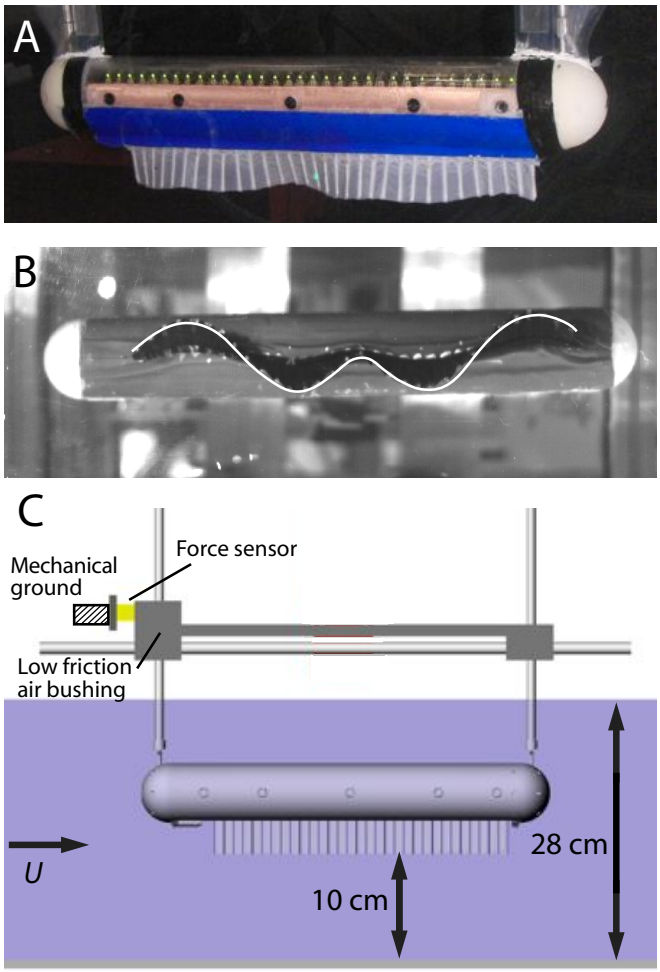

Fig. 3. Biomimetic knifefish robot and experimental setup. (A) The knifefish robot has a ventral ribbon-fin (white) to emulate the fin of knifefish such as *Eigenmannia*. The fin consists of 32 independently controlled rays, allowing for a wide range of fin kinematics such as counter-propagating waves. (B) The bottom view of the robot shows two counter-propagating waves meeting in the middle ($L_{fin}/\lambda = 2$). (C) The robot was mounted on a near-frictionless air table and suspended into a flow tunnel. A force sensor between the robot carriage and mechanical ground transduced longitudinal (fore-aft) force generated by the robot. Flow speed U was set at a constant rate from 0 to 10 cm/s depending on the experiment.

For the second experiment, we fixed the nodal point to be 0 (in the middle of the fin with $L_{\text{head}} = L_{\text{tail}}$, Fig. 1(B)) and measured longitudinal force over trials of varying flow speed. The steady state flow speed was varied from 0 to 10 cm/s increments of 0.5 cm/s. Similar to the first experiment, the experiment was repeated over a range of fin oscillation frequencies and angular amplitudes (Table II). In all robotic experiments, three replicates of data were collected.

III. RESULTS

A. Biological results

1) Nodal point varies linearly with swimming speed: Nodal shift as a function of steady state flow speed is shown in Fig. 2(C). For simplicity, the average over three replicates of data is shown for each individual and standard deviation are not shown. Nodal shift increases with respect to steady state flow speed, which means that nodal point moves toward the tail along the fin. Based on experimental observation, nodal shift seems to be a kinematic parameter that fish actively control for modulating ribbon-fin force.

TABLE I

FIN KINEMATIC PARAMETERS FOR FORCE MEASUREMENT IN THE FIRST ROBOTIC EXPERIMENT.

Experimental set	f (Hz)	θ (deg)	# waves (L_{fin} / λ)
Set 1	1, 2, 3, 4	30	4
Set 2	3	20, 25, 30	4

TABLE II

FIN KINEMATIC PARAMETERS FOR FORCE MEASUREMENT IN THE SECOND ROBOTIC EXPERIMENT.

Experimental set	f (Hz)	θ (deg)	# waves (L_{fin} / λ)
Set 1	1, 2, 3, 4	20	4
Set 2	3	20, 25, 30	4

B. Robotic and computational results

1) Robotic fin "thrust" varies linearly with nodal position: Measured force generated by the robotic knifefish, as a function of fin kinematic parameters is shown in Fig. 4. The robotic fin parameters are shown in Table I and II. The number of waves (L_{fin}/λ) was 4 in all robotic experiments. This number is within the biological relevant range of 4-5.5 for the *Eigenmannia*.

In the first robotic experiment, the effect of nodal position on net force generation was investigated. The nodal point was varied with 1.63 cm (5 percent of the robotic fin length) increments from -8.15 cm to 8.15 cm. Longitudinal force was measured with no ambient flow. Fig. 4(A-B) shows that net force generated by counter-propagating waves changes roughly linearly as a function of the nodal position along the fin. From Fig. 4(A) we observe that the slope of the force as a function of ΔL increases with the temporal frequency of the traveling waves. We define κ, *nodal shift gain*, as

$$\kappa = \frac{F}{\Delta L}. \tag{8}$$

Here, κ can be computed by fitting a linear curve to the results of Fig. 4(A-B) as the generated forces are changing linearly with respect to nodal shift. Fig. 4(A-B) reveal that *nodal shift gain* increases as the frequency and maximum angular deflection increase. The measured force from robotic experiment and the force predicted by the computational model (using the kinematic parameters from the robotic experiment) are shown in Fig. 4(C). For clarity in the comparison, only the results corresponding to θ=30° and f=3 (Hz) are shown. Although the force predicted by simulation underestimates the force measured from the robotic experiment, the trends are similar.

2) Effective "damping" force varies linearly with flow speed: In the second robotic experiment, we fixed the nodal point at 0 (thus two waves have the same length) and varied

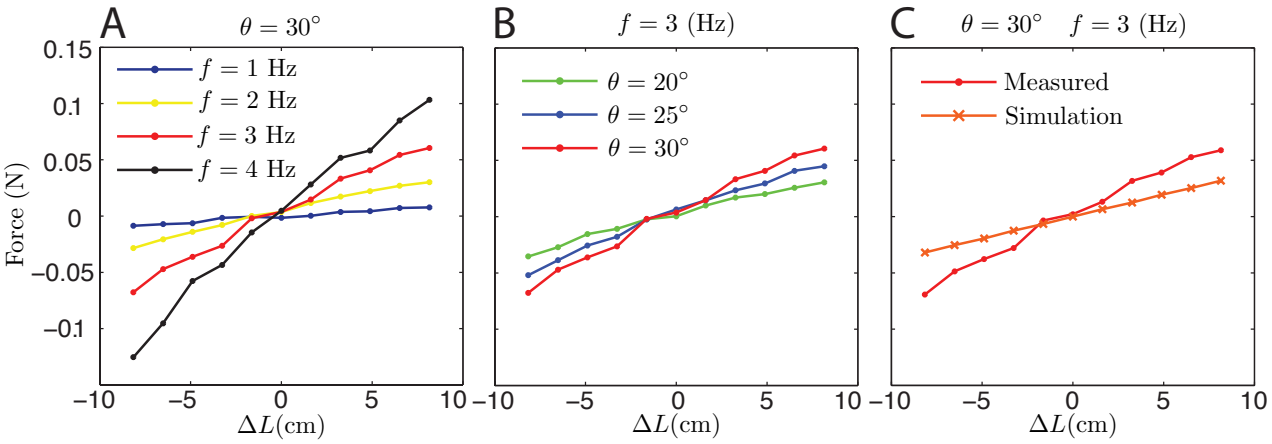

Fig. 4. Measured forces as a function of nodal shift (ΔL). (A) Robotic results: for constant angular amplitude ($\theta = 30°$), forces generated by robotic fin is shown for different frequencies. (B) Robotic results: for constant frequency ($f = 3$ (Hz)), forces generated by robotic fin is shown for different angular amplitudes. (C) For $\theta = 30°$ and $f = 3$ (Hz), generated force by the robotic fin and predicted force by simulation are shown.

the flow speed in the tunnel. The force on the robot varies linearly as a function of the steady state flow speed, as shown in Fig. 5(A-B). For these measurements, only the robotic fin was submerged. We define B, *damping constant*, as

$$B = \frac{F}{U}, \tag{9}$$

The damping constant can be computed by fitting a line to the data in Fig. 5(A-B). Damping constant increases as the frequency and maximum angular deflection of the two waves increase. In Fig. 5(C), the force measured from the robotic setup and the force predicted by simulation are shown for θ=30° and f=3 (Hz). Again, the computationally computed damping force underestimates that from robotic setup, but it nevertheless captures the linear trend.

In both the first and second experiments with the robot, each trial was repeated three times; the averages of these measurements are shown in Figs. 4 and 5.

IV. DISCUSSION

A. Maneuverability

Previously, Curet *et al.* [5] showed that the surge (fore-aft) force increases nonlinearly as a function of frequency and angular amplitude when there is only one single traveling wave along the fin. Using the computational model in this study, Fig. 6 shows a comparison between the thrust that would be produced by counter-propagating waves versus that of a single traveling wave along the fin. From Fig. 6(A) we observe that generated thrust force is changing linearly as a function of nodal shift as we saw the result from robotic experiment in previous section. Fig. 6(B-C) shows that the surge force increases nonlinearly as a function of frequency and angular amplitude with a single traveling wave as the primary propulsion mechanism. Negative frequency and negative angular amplitude indicate that the wave direction along the fin is reversed thus the force is negative—as would be required to accelerate the fish in the opposite direction.

There may be a significant maneuverability (and control authority) advantage to using counter-propagating waves, compared to using a single traveling wave. A single traveling wave leaves a "dead-band" effect for thrust generation. This is because, when hovering (near zero net force), small changes in force require large and rapid reversals in the fin wave direction, since the slope of the curves in Fig. 6(B-C) at the origin are zero. Counter-propagating waves, by contrast, enable the fish to generate rapid changes to fore-aft thrust easily, since the force profile is linear as a function of ΔL. Note that the vertical scales on Fig. 6 are the same, and the abscissas are all in the biologically and robotically relevant ranges. Hence the counter-propagating wave strategy enhances the maneuverability of fish for changing the direction, as would be required for closed-loop stable control in the face of perturbations.

B. Stability

Counter-propagating waves provide "linear damping", similar to the flapping counter-torque (FCT) mechanisms proposed as a mechanism employed by high-frequency flapping fliers [8]. As depicted in Fig. 5, the net force over the fin increases linearly as a function of steady state flow speed.

Enhanced maneuverability and stability are provided at the expense of energy since the fish produce antagonistic counter-propagating waves even when the fish is hovering. Depending on the task at hand, this energetic expenditure may be worth the added benefits we have shown in this paper.

V. ACKNOWLEDGMENTS

This material is based upon work supported by NSF under grants 0941674 and 0845749, and ONR under grant N000140910531. We thank James Snyder (Northwestern University) for embedded LUA programming and assistance with other aspects of running the robot experiments.

REFERENCES

[1] T. Benson. Shape effects on drag. http://wright.nasa.gov/airplane/shaped.html, 2004.
[2] N. S. Bernstein. *The coordination and regulation of movements*. Pergamon, Oxford, 1967.

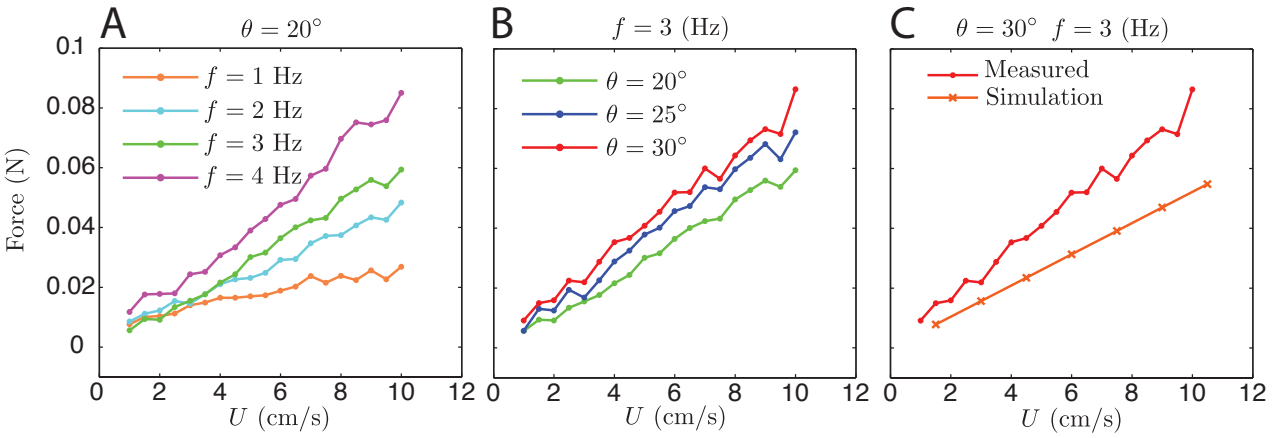

Fig. 5. Measured forces on the robotic fin as a function of steady state flow speed (U). (A) Robotic results: for constant angular amplitude ($\theta = 20°$), forces acting on the robotic fin is shown for different frequencies. (B) Robotic results: for constant frequency ($f = 3$ (Hz)), forces acting on the robotic fin is shown for different angular amplitudes. (C) For $\theta = 30°$ and $f = 3$ (Hz), forces acting on the robotic fin and predicted force by simulation are shown.

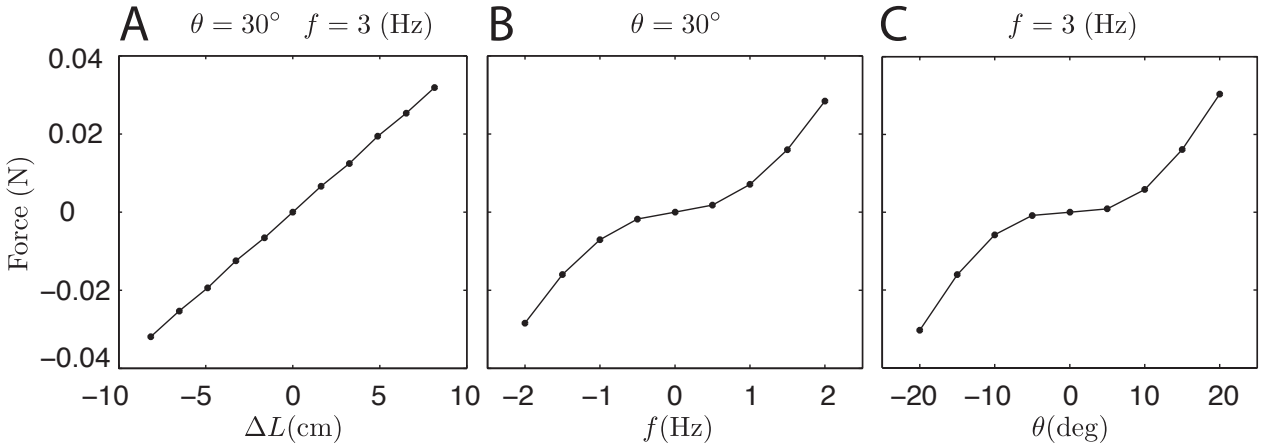

Fig. 6. Comparison of thrust generation by varying only one kinematic parameter predicted by simulation. (A) Generated force is changing linearly as a function of nodal position. Nodal point is exactly in the middle of the fin when $\Delta L = 0$. (B) Generated force by a single traveling wave along the fin as a function of wave frequency. Negative frequency means wave direction is reversed. The fin does not move when $f = 0$. (C) Generated force by a single traveling wave along the fin as a function of angular amplitude. Negative angular amplitude means wave direction is reversed. The fin does not move when $\theta = 0$.

[3] N. J. Cowan and E. S. Fortune. The critical role of locomotion mechanics in decoding sensory systems. *J. Neurosci.*, 27(5):1123–1128, 2007.

[4] O. M. Curet, N. A. Patankar, G. V. Lauder, and M. A. MacIver. Aquatic manoeuvering with counter-propagating waves: a novel locomotive strategy. *Journal of the Royal Society Interface*, 8(60):1041–1050, 2011.

[5] O. M. Curet, N. A. Patankar, G. V. Lauder, and M. A. MacIver. Mechanical properties of a bio-inspired robotic knifefish with an undulatory propulsor. *Bioinspiration & Biomimetics*, 6(2):026004, 2011.

[6] O. Ekeberg. A combined neuronal and mechanical model of fish swimming. *Biological Cybernetics*, 69(5-6):363–374, Oct. 1993.

[7] T. L. Hedrick. Software techniques for two-and three-dimensional kinematic measurements of biological and biomimetic systems. *Bioinspiration & biomimetics*, 3:034001, 2008.

[8] T. L. Hedrick, B. Cheng, and X. Y. Deng. Wingbeat Time and the Scaling of Passive Rotational Damping in Flapping Flight. *Science*, (5924):252–255+.

[9] A. Hitschfeld, S. Stamper, K. Vonderschen, E. Fortune, and M. Chacron. Effects of restraint and immobilization on electrosensory behaviors of weakly electric fish. *ILAR J.*, 50(9), 2009. In press.

[10] J. Lighthill and R. Blake. Biofluiddynamics of balistiform and gymnotiform locomotion. part 1. biological background, and analysis by elongated-body. *Journal of Fluid Mechanics*, 212:183–207, 1990.

[11] M. A. MacIver, N. A. Patankar, and A. A. Shirgaonkar. Energy-information trade-offs between movement and sensing. *PLoS Computational Biology*, 6(5):e1000769, 05 2010.

[12] K. A. McIsaac and J. P. Ostrowski. A geometric approach to anguilliform locomotion: Modelling with an underwater eel robot. In *ICRA*, pages 2843–2848, 1999.

[13] G. J. Rose and J. G. Canfield. Longitudinal tracking responses of *Eigenmannia* and *Sternopygus*. *J. Comp. Physiol. A*, 173:698–700, 1993.

[14] E. Roth, K. Zhuang, S. A. Stamper, E. S. Fortune, and N. J. Cowan. Stimulus predictability mediates a switch in locomotor smooth pursuit performance for *Eigenmannia virescens*. *J. Exp. Biol.*, 214(7):1170–1180, Apr 2011.

[15] M. Sfakiotakis, D. M. Lane, and J. B. C. Davies. Review of fish swimming modes for aquatic locomotion. *IEEE J. Ocean. Eng.*, 24(2):237–252, 1999.

[16] M. Sfakiotakis and D. P. Tsakiris. SIMUUN : A simulation environment for undulatory locomotion. *International Journal of Modelling and Simulation*, 26:350–358, 2006.

[17] S. A. Stamper, E. Roth, N. J. Cowan, and E. S. Fortune. Active sensing via movement shapes spatiotemporal patterns of sensory feedback. *J. Exp. Biol.*, 2012. Accepted.